Journal of Magnetic Resonance **150,** 214–218 (2001)
doi:10.1006/jmre.2001.2347, available online at http://www.idealibrary.com on IDEAL®

COMMUNICATIONS

Nuclear Relaxation Time Images by Radiofrequency Field Gradients Applied to the Study of Solvent Permeation into Polymeric Materials

C. Malveau, D. Grandclaude, and D. Canet[1]

Laboratoire de Méthodologie RMN, UPRESA CNRS 7042, FR CNRS 1742 (INCM), Université H. Poincaré, BP 239, 54506 Vandoeuvre-les-Nancy Cedex, France

Received October 27, 2000; revised March 26, 2001; published online May 10, 2001

T_2 images are obtained by two interleaved B_1-gradient imaging experiments preceded by CPMG trains of different lengths. The method is assessed by means of a phantom involving compartments of different, though relatively close, T_2 values. T_1 images arise from a previously published procedure also based on two interleaved B_1-gradient imaging experiments involving different evolution of the longitudinal magnetization. Both types of image appear to be useful in view of the structural characterization of polymer samples through the T_2 and T_1 distribution of a solvent embedded in the material.

Most NMR images are inherently contrasted by the action of spin relaxation during the experiment (*1*). However, obtaining accurate relaxation time values (T_1 or T_2) in the third dimension (instead of the spin density) may be less straightforward, especially in the case of biological tissues (*2, 3*). We are mostly interested here in the determination of transverse relaxation times (T_2). They can be mapped by performing a pixel-by-pixel analysis of the images acquired with different values of the echo time in a pulsed field gradient (PFG) spin-echo sequence. However, diffusion processes may heavily affect the T_2 values (*4*) and different methods have been proposed to circumvent this problem. One of them, which concerns the spin–echo imaging sequence, consists of placing the phase gradient pulse immediately before the read gradient in such a way they do not form a PFG sequence (*5*); another one makes use of a preparation period of the CPMG (Carr Purcell Meiboom Gill) (*6, 7*) type which precedes the spin–echo sequence in such a way that the effects of T_2 relaxation and diffusion are uncoupled by the fact that the echo time remains constant (*8*). These methods make use of static magnetic field gradients (B_0 gradients) and suffer from the limitations inherent in such gradients (e.g., magnetic field inhomogeneity effects and magnetic susceptibility variations inside the sample (*9, 10*)).

Some time ago, we devised a method based on radiofrequency field gradients (B_1 gradients) and on the SUFIR (super fast inversion recovery (*11*)) experiment with the goal of obtaining spatially resolved longitudinal relaxation times (T_1) (*12*). This was motivated by the fact that B_1 gradients are not hampered by the problems encountered when using B_0 gradients, whereas SUFIR employs only two experiments for accurately determining T_1 and thus requires a minimal measuring time. Along the same lines, we present in this paper a method for the spatial determination of transverse relaxation times; it involves a combination of the CPMG experiment and the imaging procedures by radiofrequency field gradients currently in use in this laboratory (*13*). The main idea relies on the comparison of a reference image (S_1) and a partially relaxed image (S_2), both experiments being interleaved. The measuring time is thus reduced with respect to the classical methods which involve the repetition of the imaging experiment for several values of some interval sensitive to the relaxation time and subsequently, the analysis of the evolution curve for each pixel. The accuracy of the proposed method will be checked with phantoms and shown to be adequate so as to perform a meaningful analysis of transverse relaxation of a solvent inside a polymeric material. Concerning this latter issue, we shall supplement T_2 images by T_1 images in order to assess the characterization of anisotropic versus isotropic polymeric materials. The interpretation of the different features of both types of image will be shown to be consistent and complementary.

To render the CPMG experiment space dependent, the normal fid acquisition is replaced by a train of short B_1 gradient pulses with acquisition of a single point between two consecutive pulses (Fig. 1). The Fourier transform of the pseudo-fid which has been obtained that way yields the spatial profile of the projection upon the B_1 gradient direction (*14*). A 2D map is obtained by a step-by-step sample rotation and a treatment based on the projection–reconstruction principle along with an adaptation of the "filtered back projection" algorithm (*13*). A pixel-by-pixel analysis leads to the required T_2 map, assuming only one T_2 for each pixel. The

[1] To whom correspondence should be addressed.

1090-7807/01 $35.00

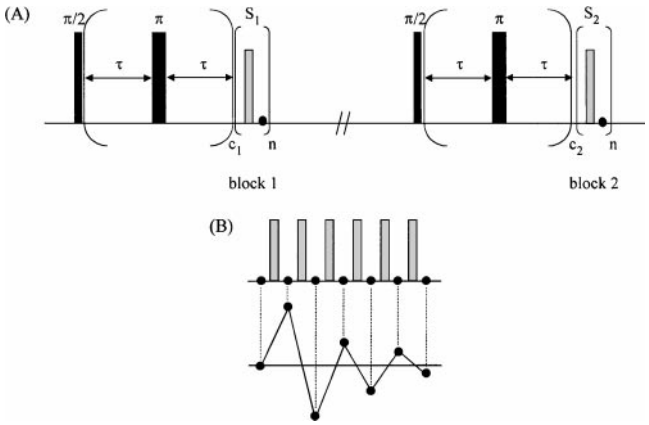

FIG. 1. (A) Scheme of the sequence used for the spatial determination of T_2; it stems from the comparison of a reference image (S_1) and a partially relaxed image (S_2). c_1 and c_2 correspond to the numbers of loops for the reference and relaxed spectra, respectively. Solid rectangles correspond to rf (radiofrequency) pulses assumed to be homogeneous (acting in the same way at any location in the object under investigation), whereas shaded rectangles stand for rf gradient pulses. (B) Principle of the imaging procedure employing a radiofrequency field gradient. The gradient is applied in the form of a pulse train, with acquisition of a single data point between two consecutive pulses.

alternate block acquisition mode affords compensation for any instrumental drift, and T_2 can then be accurately obtained by

$$T_2 = \frac{-2\tau(c_2 - c_1)}{\ln(I_2/I_1)}, \qquad [1]$$

where I_1 and I_2 are the signal intensities in blocks 1 and 2, respectively, and τ the time interval of the CPMG pulse train (see Fig. 1). The retained pixels are those for which the intensity in the reference image (block 1) is greater than a threshold value defined by the user (above the noise level). If, by chance, a pixel intensity in the partially relaxed image would be greater than the one in the reference image, the corresponding T_2 would be set to zero. In practice, such a situation was never (or scarcely) met. Nevertheless, this was included as a safeguard in the automatic procedure for producing T_2 images. Moreover, if the T_2 value found for a given pixel is outside the expected range, it will be also set to zero. The first test was carried out with a phantom made of three capillaries containing water with different amounts of copper sulfate so that the corresponding transverse relaxation times (measured separately by the CPMG method for each capillary) are 330, 250, and 370 ms, respectively. As shown in Fig. 2, the results of the imaging experiment are especially clean, the limits of the capillaries are well defined, and the T_2-based discrimination appears convincing. It can be especially noticed that Eq. [1] could be applied to *all* pixels within each capillary. The noise at the top of each cylinder is representative of the accuracy with which T_2 is determined and is seen to lie in a somewhat narrow range, so that the capillaries for which the T_2 values differ by about 10% are differentiated quite unambiguously. In Table 1 are reported the average and T_2 extreme values for each capillary along with the standard deviations calculated over all pixels defining each capillary; the latter provide an estimation of the experimental uncertainty which can be seen to be $\pm 1\%$.

TABLE 1
Transverse Relaxation Times (in ms) of the Sample Made of Three Capillaries

Method	"Classical" T_2	Imaging T_{2ave}	Imaging T_{2min}	Imaging T_{2max}	Imaging σ
Capillary 1	330	332	314	350	8.0
Capillary 2	250	247	234	256	4.1
Capillary 3	370	376	354	389	7.5

Note. Data have been obtained by the classical method (CPMG) and by the proposed imaging experiment described here. T_{2min} and T_{2max} are the extreme values, whereas T_{2ave} is the average value and σ is the standard deviation. These two latter quantities have been calculated over all the pixels defining a capillary.

The second example (Fig. 3) is more directed toward possible applications and concerns a solvent (toluene) within a polymeric material (high-density polyethylene, HDPE). Two types of samples (in the form of parallelepipedic bars) were prepared:

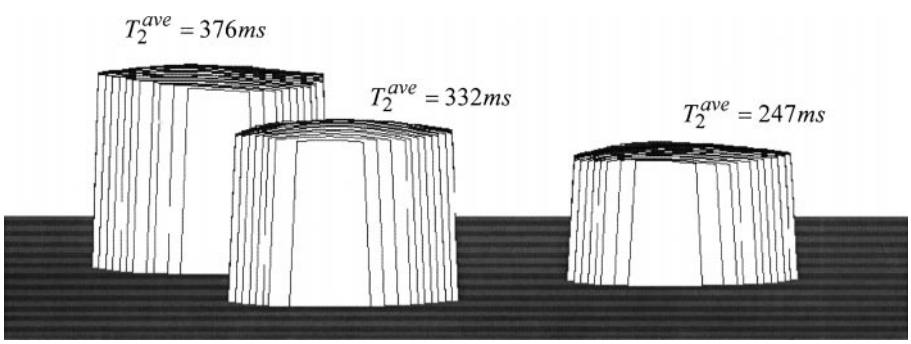

FIG. 2. T_2 map of three capillaries containing water doped with different amounts of copper sulfate (T_2^{ave} is the average value calculated over all the pixels of the considered capillary). τ, c_1, and c_2 were set to 400 μs, 2, and 500, respectively (see Fig. 1A). Two-dimensional images were obtained by rotating the sample in 3.6° steps. ^{1}H measurements were performed at 100 MHz with a probe delivering a B_1 gradient of 46 gauss cm^{-1} (sample temperature: 25°C).

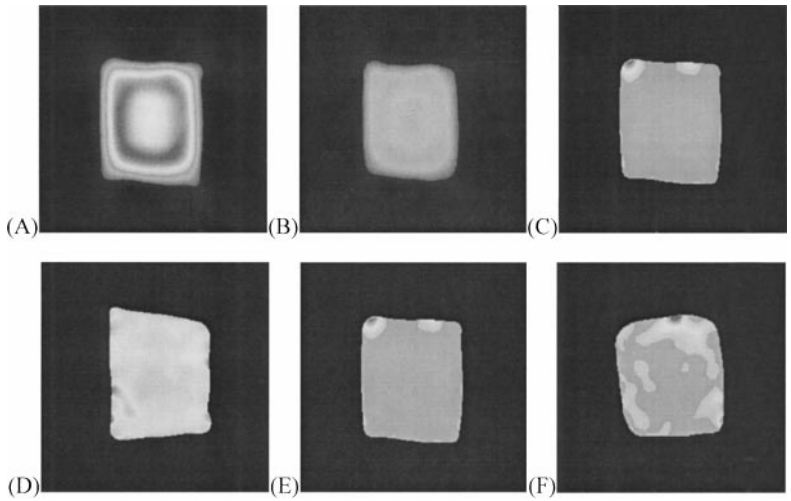

FIG. 3. Toluene within HDPE (high density polyethylene) samples. τ, c_1, and c_2 were set to 100 μs, 2, and 80, respectively (see Fig. 1A). The two-dimensional images were obtained by rotating the sample in 1.8° steps. Pixel by pixel comparison of reference (A) and partially relaxed (B) images yields the T_2 map (C). These images correspond to an "anisotropic" sample of HDPE (see text) which has been immersed in toluene for 30 h. The three lower images are T_2 maps corresponding respectively to "isotropic" (D) and "anisotropic" (E) HDPE (both after immersion time of 30 h) and to the "anisotropic" sample at saturation (F). Immersion and NMR experiment temperature: 25°C.

(i) One is referred to as "isotropic" because it has been cut from the core material (spherolitic polyethylene), all sides being in principle identical.

(ii) The other sample is denoted "anisotropic," its sides differing two by two, because it has been cut from a plate and not from core material. Two opposite sides correspond to the original surfaces of the plates in contact with the injection mold and are known to possess a skin of ca. 30 μm with transcrystalline morphology (crystalline lamellae aligned along the direction perpendicular to the surface). The other two opposite sides were cut in the bulk of the plates and correspond to the core material.

These bars were immersed in liquid toluene. The solvent migrates faster through the surfaces that have been in contact with the injection mold, presumably due to the particular properties of the skin mentioned above.

We have obtained T_2 maps for each sample and for two immersion times (30 h and saturation). These maps correspond exclusively to toluene within the polymeric material, the huge linewidths of the latter precluding any significant contribution to images obtained by the experimental procedures used here. In spite of spin density images clearly exhibiting a heterogeneity of toluene concentration (shortage of toluene can be seen at the center of the sample, Figs. 3A and 3B), the T_2 map is much more uniform (Fig. 3C), indicating that toluene transverse relaxation time is quasi-constant, regardless of the actual concentration at a given location within the sample. This feature is indeed observed for the two samples after an identical immersion time (30 h, Figs. 3D and 3E); concerning the anisotropic sample at saturation (Fig. 3F), some variations (though in a narrow range) are visible but they do not appear to be correlated with the specificity of this sample (two sides having been in contact with the injection mold). In fact, the three T_2 images (3C–3E) have not been normalized, so that deceptive large variations can be ascribed to a small difference between the highest and lowest pixel intensities.

Indeed, differences in T_2 values observed in each map which, although small, are significant with regard to the experimental uncertainty, cannot, at first sight, be associated with any morphological property. It must however be borne in mind that a given pixel encompasses a very large area at the macromolecular scale and thus can be representative of several different structural features (e.g., amorphous, crystalline, oriented, . . .) with unpredictable proportions (and possibly varying randomly from one experiment to the other). As suggested by Kuhn *et al.* (*15*) in another context, we have thus represented the distribution of toluene transverse relaxation times in the form of histograms (Fig. 4) and subsequently fitted this distribution according to gaussian functions with the hope of gaining some insight into the structural properties of the polymer sample. We can notice a strong asymmetry (involving two well-characterized gaussian functions) for "anisotropic" HDPE after an immersion time of 30 h. (Fig. 4B), whereas essentially a single gaussian function described the T_2 distribution in the "isotropic" sample after the same immersion time (Fig. 4A); this is also true for "anisotropic" HDPE at saturation (Fig. 4C). For these two latter samples, the distribution exhibits nearly the same shape. We can explain the asymmetric distribution of T_2 in "anisotropic" HDPE by the particular structure of the two sides involving a skin as described above. When toluene penetrates the polymer by the skin (and solvent uptake occurs preferentially that way), its environment is more organized and the fact that T_2 is smaller can be explained by the unique property of transverse relaxation rates, which are dominated by spectral densities at zero frequency if

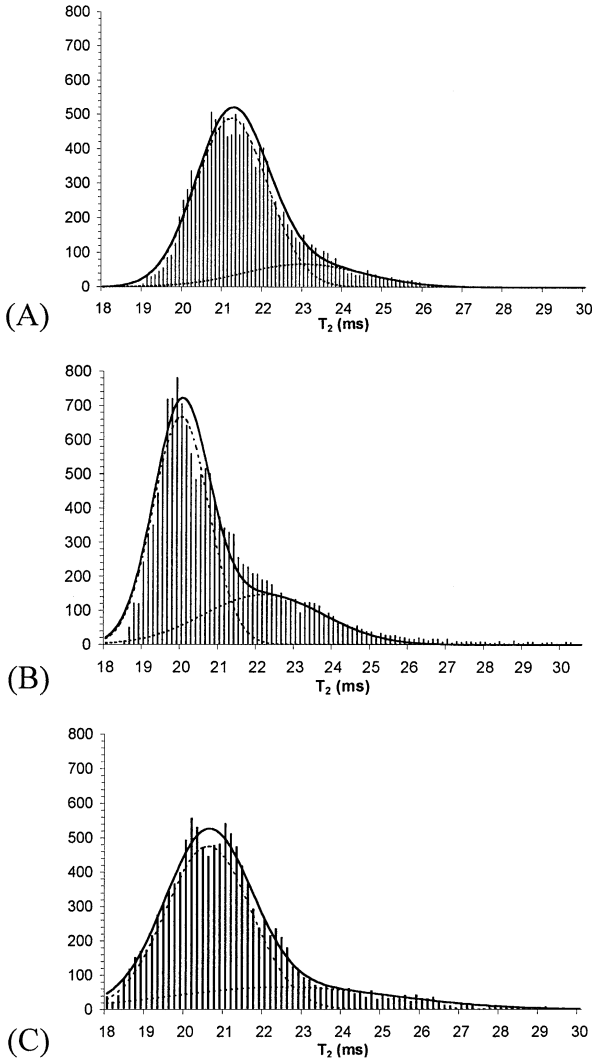

FIG. 4. Distribution of the transverse relaxation time of toluene within "isotropic" (A) and "anisotropic" (B) HDPE after immersion time of 30 h and within the "anisotropic" sample at saturation (C) (corresponding to Fig. 3D, 3E, and 3F, respectively).

slow motions are present (this is certainly the case here due to the interaction of the solvent with the polymeric matrix), and by relying on a simple model such as the one of Lipari and Szabo (*16*), which yields

$$\frac{1}{T_2} \approx K \tau_c S^2, \qquad [2]$$

where K is a scaling factor related to the interactions affecting the toluene protons, τ_c a correlation time associated with slow motions, and S an order parameter which increases with the degree of organization. Indeed, as already mentioned, Fig. 4B reveals that two distributions exist for the "anisotropic" sample after 30 h of immersion: the minor one, centered around 21 ms, is similar to the predominant distribution in the "isotropic" sample after the same immersion time (Fig. 4A) and would be assigned to toluene in the core material; the major one involves a shorter T_2 (centered around 19.5 ms) and would correspond to more organized regions of the material, which are preferentially present in the "anisotropic" sample. Of course, after a long time of immersion, this organization tends to decrease due to swelling processes and a situation analogous to that of the "isotropic" sample is retrieved (this can be appreciated by comparison of Figs. 4C and 4A).

In order to assess and possibly complement the relaxation time approach for material characterization, we have run T_1 imaging experiments according to the method above mentioned (*12*) (thus, no further explanation needs to be given). Experimental conditions are identical to those prevailing for T_2 images and will not be repeated. Again, we had recourse to histograms which are displayed in Fig. 5. As can be observed, the "isotropic" sample after an immersion time of 30 h as well as

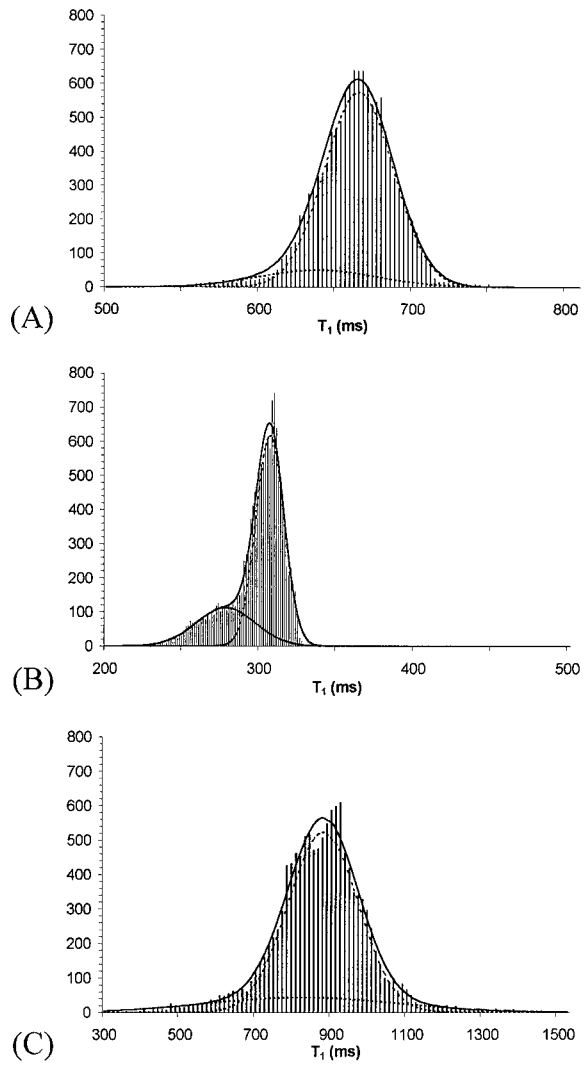

FIG. 5. Distribution of the longitudinal relaxation time of toluene within the same samples and with the same conditions of immersion as in Fig. 4.

the "anisotropic" sample at saturation exhibit a single gaussian distribution. By contrast, two distinct gaussian distributions are clearly visible for the "anisotropic" sample after 30 h of immersion. In this respect, it appears that discrimination of the two types of sample is possible from symmetry (or dissymmetry) of T_1 distribution, as this was done for T_2 distributions. However, the values found for longitudinal relaxation times, as well as the location of the minor distribution with respect to the major one (when two distributions exist), require some further interpretation, especially with reference to the distribution of transverse relaxation times. It must be borne in mind that, as far as longitudinal relaxation times are concerned, fast motions become predominant whenever they coexist with slower motions (those described by correlation times on the order of 1 ns or larger). This is due to the fact that longitudinal relaxation rates involve spectral densities at the measurement frequency and at twice this frequency, in such a way that the contribution from slow motions essentially vanishes. Consequently, one is left with fast rotational motions which depend mainly on the size and on the nature of the cavities in which the solvent molecules are moving. These cavities being related to swelling processes, we can conceive that they are smaller or of different shapes in the more organized part of the material, thus inducing some hindrance of the fast motions and yielding smaller T_1 (see the minor contribution in Fig. 5B, which concerns the "anisotropic" sample). Also, for this sample, we can easily accept that swelling proceeds more slowly and that cavities are consequently smaller; this explains that T_1 are globally smaller than for the "isotropic" sample (compare Figs. 5A and 5B). Finally, it can be noticed that T_1 distributions are much broader than T_2 distributions, indicating a sort of polydispersity of cavities (or channels).

We have proposed a simple experiment yielding accurate T_2 images in a measuring time roughly twice that required for a conventional spin density image. We have performed this experiment on a solvent inside polymeric samples of industrial interest and shown that, although the images themselves do not exhibit any correlation with the structural properties of the material, the T_2 distribution over all the voxels provides interesting information. When samples are homogeneous, either naturally or subsequent to swelling, this distribution is essentially accounted for by a single gaussian function. Conversely, for an "anisotropic" sample, two gaussian functions are necessary, one of them corresponding to more organized regions of the sample. These findings are confirmed by the T_1 distributions obtained from complementary experiments. However, comparison of T_2 and T_1 results and their interpretation require the consideration of different types of motions affecting solvent molecules within a polymeric material. These results appear consistent if it is realized that T_2 is dominated by slow motions whereas T_1 depends only on fast motions. Both types of motion are superimposed; the former arises from interaction of solvent molecules with the polymer while the latter corresponds to reorientation of solvent molecules inside the cavities or channels which have been created in the swelling process.

REFERENCES

1. W. S. Price, NMR imaging, *Ann. Rep. NMR Spectrosc.* **35,** 139–216 (1998).
2. P. A. Bottomley, C. J. Hardy, R. E. Argersinger, and G. Allen-Moore, A review of ^{1}H nuclear magnetic resonance relaxation in pathology: Are T_1 and T_2 diagnostic? *Med. Phys.* **14,** 1–37 (1987).
3. S. Lüsse, H. Claasen, T. Gehrke, J. Hassenpflug, M. Schünke, M. Heller, and C.-C. Glüer, Evolution of water content by spatially resolved transverse relaxation times of human articular cartilage, *Magn. Reson. Imaging* **18,** 423–430 (2000).
4. M. Brandl and A. Haase, Molecular diffusion in NMR microscopy, *J. Magn. Reson. B* **103,** 162–167 (1994).
5. E. W. Hsu, J. S. Schoeniger, R. Bowtell, N. R. Aiken, A. Horsman, and S. J. Blackband, A modified imaging sequence for accurate T_2 measurements using NMR microscopy, *J. Magn. Reson. B* **109**, 66–69 (1995).
6. H.Y. Carr and E.M. Purcell, Effects of diffusion on free precession in nuclear magnetic resonance experiments, *Phys. Rev.* **94,** 630–638 (1954).
7. S. Meiboom and D. Gill, Modified spin–echo method for measuring nuclear relaxation times, *Rev. Sci. Instrum.* **29,** 688–691 (1958).
8. A. Haase, M. Brandl, E. Kuchenbrod, and A. Link, Magnetization-prepared NMR microscopy, *J. Magn. Reson. A* **105,** 230–233 (1993).
9. R. Raulet, J. M. Escanyé, F. Humbert, and D. Canet, Quasi-immunity of B_1 gradient NMR microscopy to magnetic susceptibility distortions, *J. Magn. Reson. A* **119,** 111–114 (1996).
10. W. S. Price, Gradient NMR, *Annu. Rep. NMR Spectrosc.* **32,** 51–142 (1996).
11. D. Canet, J. Brondeau and K. Elbayed, Superfast T_1 determination by inversion-recovery, *J. Magn. Reson.* **77,** 483–490 (1988).
12. F. Humbert, E. Collenne, M. Valtier, and D. Canet, Nuclear longitudinal relaxation time images by radiofrequency field gradients, *J. Magn. Reson.* **138,** 164–166 (1999).
13. P. Maffei, P. Mutzenhardt, A. Retournard, B. Diter, R. Raulet, J. Brondeau, and D. Canet, NMR microscopy by radiofrequency field gradients, *J. Magn. Reson. A* **107,** 40–49 (1994).
14. D. Canet, Radiofrequency field gradient experiments, *Progr. NMR Spectrosc.* **30,** 101–135 (1997).
15. W. Kuhn, P. Barth, S. Hafner, S. Simon, and H. Schneider, Material property NMR imaging of cross-linked polymers by NMR, *Macromolecules* **27,** 5773–5779 (1994).
16. G. Lipari and A. Szabo, Model-free approach to the interpretation of nuclear magnetic resonance relaxation in macromolecules, *J. Am. Chem. Soc.* **104,** 4546–4570 (1982).